RESEARCH ARTICLE

LASER & PHOTONICS REVIEWS

www.lpr-journal.org

Achieving Broadband Near-Field Directionality with a 3D Active Janus Antenna

*Bo Xue, Kayode Adedotun Oyesina, and Alex M. H. Wong**

Directional sources like the Huygens source enable electromagnetic wavefront forming/shaping with great flexibility and have made impacts in photonics, applied physics, metasurfaces, and antenna engineering. The related Janus source features a strongly directional near-field and a quasi-isotropic far-field, which gives it promising application potentials distinct from, and complementary to, the Huygens source. Nevertheless, most existing Janus sources face strong limitations in efficiency and/or 3D operation, hindering their practical application. This paper introduces a 3D active Janus source that achieves near-field directionality over a wide bandwidth and a power efficiency much improved over existing passive Janus sources. It is shown that a class of quasi-isotropic antennas are actually active Janus sources (which is referred to as the Janus antenna). A well-designed Janus antenna is demonstrated which (a) exhibits near-field directionality over a broad bandwidth of 28.9%, and (b) in a practical usage environment, achieves a power efficiency ≈60 times higher than a passive Janus source. This work elucidates the connection between the "Janus dipole" concept in physics and the "quasi-isotropic antenna" concept in antenna design, and paves the way for the design of future directional devices with much improved bandwidth and efficiency.

1. Introduction

Recent progresses on directional dipoles, from optics to microwaves, are of immense interest. Particularly, near-field directional dipoles assume an important role in building future compact directional systems. Ref.[1] introduces three fundamental directional dipoles: the circular dipole, the Huygens dipole, and the Janus dipole. These three dipoles' near-field directionalities are exhibited through the spin, the real part of the Poynting vector, and the imaginary part of the Poynting vector, respectively.[1] In particular, the Huygens and Janus sources are similarly constructed, consisting of orthogonal electric and magnetic dipoles, which radiate in phase for the Huygens source and 90° out of phase for the Janus source. The Huygens source is directional in both the near-field and the far-field. This property finds application in diverse realms, including the design of directional devices,[2,3] high gain antennas,[4–6] and Huygens metasurfaces.[7,8] On the other hand, while the Janus source is quasi-isotropic in the far-field, it possesses a unique near-field directionality which has been investigated and demonstrated in numerous studies.[1,9–23] These characteristics position the Janus source as a promising candidate for the design of compact directional devices. Controlling its near-field directionality, the Janus source also has the potential to build future compact multiple-input and multiple-output (MIMO) systems with weak near-field inter-element coupling as well as far-field quasi-isotropy, and wireless transmission systems with strong inter-element coupling. We note that the term "Janus" is also used in metasurface research to refer to a category of two-faced 2D metamaterials with different front and back transmission properties.[24–27] While these Janus metasurfaces also achieve various bidirectional asymmetric properties, the Janus source in this work refers specifically to a class of dipole constructed by orthogonal electric and magnetic dipoles with a 90-degree phase difference, showing a strong directional preference in near-field power coupling.

Figure 1 shows representative works on Janus sources, grouped into three categories according to how the source is modeled and/or implemented. We shall classify these sources as the theoretical source,[1,9] the passive source,[10,11,13,15,18,20] and the recently proposed 2D active source.[22] The theoretical sources[1,9] study the Janus dipole as a pair of ideal, infinitesimal electric and magnetic currents that are co-located, orthogonally oriented, and 90° out of phase. While useful in theoretical studies, they cannot be directly implemented in a physical device. Passive sources are particles such as nanospheres,[10] acoustic cylinders,[11,13] dolmen,[15] dielectric cylinders,[18] and helices,[20] which can be carefully designed such that when they scatter an

B. Xue, K. A. Oyesina, A. M. H. Wong
Department of Electrical Engineering
City University of Hong Kong
Hong Kong 999077, China
E-mail: alex.mh.wong@cityu.edu.hk

A. M. H. Wong
State Key Laboratory of Terahertz and Millimeter Waves
City University of Hong Kong
Hong Kong 999077, China

The ORCID identification number(s) for the author(s) of this article can be found under https://doi.org/10.1002/lpor.202401093

DOI: 10.1002/lpor.202401093

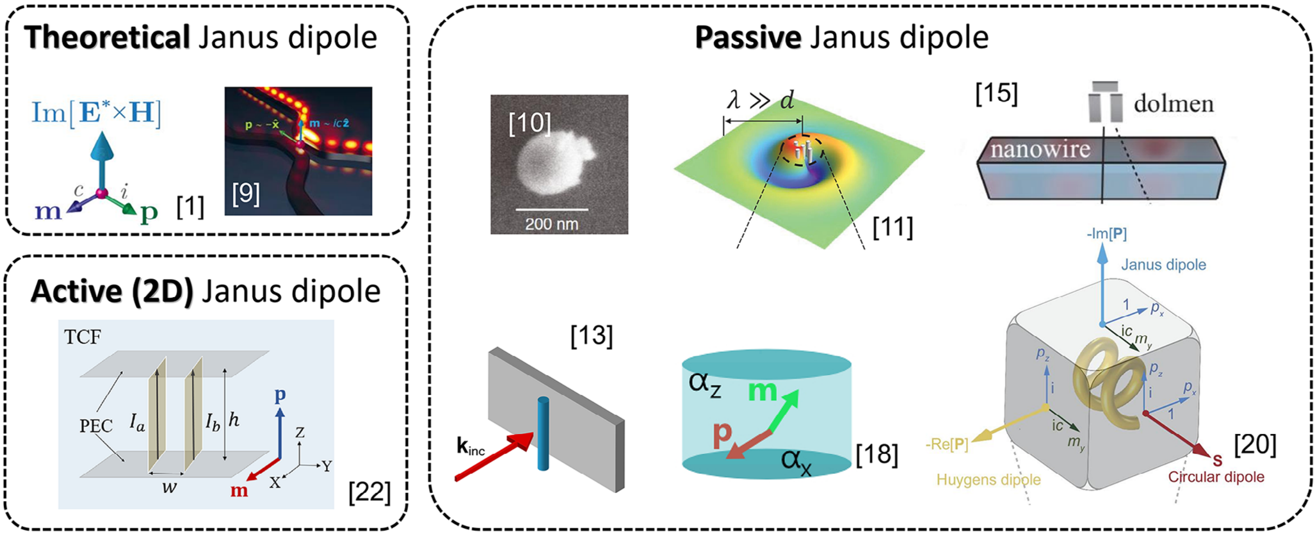

Figure 1. Some examples of the theoretical Janus source,[1,9] the passive Janus source,[10,11,13,15,18,20] and the recently proposed 2D active Janus source.[22] For Refs. [1] and [15]: Copyright obtained from the American Physical Society.

incoming plane wave from a desired direction and polarization, they generate a secondary source which is Janus in character. Although these sources are conceptually viable, the particles only re-scatter a very small part of the incident wave, leading to very low power efficiency. Further, the re-scattering amplitude and phase of the electric and magnetic dipoles are carefully optimized for a single frequency, leading to single-frequency and/or narrow-banded operation. In recent works, we have proposed an active 2D Janus source within a parallel plate waveguide,[19,22] and used it to perform investigations on near-field directionality and power coupling suppression. However, the source is confined to a 2D structure, thereby imposing limitations on its application in free space. Hence, a pressing need arises for the introduction of a 3D active Janus source. A 3D active Janus source, with strong directional control to radiation and coupling in free-space, can open immense practical application possibilities.

Notably, in the antenna community, researchers have also investigated the superposition of orthogonal electric and magnetic dipoles with 90-degree phase difference. This configuration is recognized as a "quasi-isotropic antenna" due to its characteristic of quasi-isotropic radiation pattern in the far field.[28–37] Whilst ample works have investigated the radiation characteristic of the quasi-isotropic antenna, its near-field properties and its relation with the Janus source remain heretofore unexplored.

In this paper, we perform research toward the realization of a 3D active Janus source and demonstrate its capability in near-field directional coupling. We demonstrate that a practical active source, previously recognized as a type of quasi-isotropic antenna, also possesses the strong near-field directionality one expects from a Janus source. Simulations and experiments show that the chosen Janus antenna achieves near-field directionality over a broad bandwidth of 28.9%, while the efficiency of our active Janus antenna can be improved more than 60-fold compared to using a passive Janus source. Our work bridges existing studies on the electro-magnetic dipole from the physics and antenna communities and culminates in the demonstration of a wideband and power-efficient 3D active Janus source.

2. Near-Field Coupling with Janus Antenna

The configuration of the Janus source, namely, a pair of electric and magnetic dipoles which are co-located, orthogonally oriented, of approximately equal amplitude, and 90°-phase-shifted, has long been of interest to the antenna community. This configuration of dipoles has been studied under the topic of the quasi-isotropic antenna[28–37]: it has the desirable property of radiating into all directions with near-equal strengths. Quasi-isotropic antennas of various sizes and operation mechanisms have been proposed, and their far-field radiation performances have been extensively studied. Leveraging this result, we synthesize an electrically-small quasi-isotropic antenna and demonstrate that it also has the near-field directional properties of the Janus source. We will call this the Janus antenna.

The chosen Janus antenna, first reported in,[33] achieves the necessary electric and magnetic currents using near-field resonant parasitic (NFRP) elements. As illustrated in **Figure** 2a, the antenna is composed of two radiating constituents: the metallic trace highlighted in pink forms a folded dipole, and the metallic trace highlighted in blue forms a capacitively loaded loop (CLL). An incident wave excites both elements via coupling through a coplanar stripline (CPS) section, which is highlighted in green. Through appropriate structuring of the folded dipole, CLL and CPS, orthogonal electric (**p**) and magnetic (**m**) dipoles can be generated with a ninety-degree phase difference and of the relative strengths stipulated by Equation (S3) (Supporting Information) — thus forming a Janus source. The electrical dimensions of the antenna are compact: $0.165 \times 0.164 \times 0.006\ \lambda^3$, where $\lambda = 123$ mm is the wavelength of the antenna operating at the resonant frequency of 2.43 GHz. The S11 plot, shown in Figure 2b, shows that the antenna can radiate very effectively at this frequency. In terms of far-field radiation behavior, Figure 2a shows the antenna's quasi-isotropic characteristic. The antenna has a maximum directivity of 1.4 dB and a minimal directivity of −1.2 dB. The difference between these values is within 3 dB, which aligns with the common criterion for quasi-isotropic

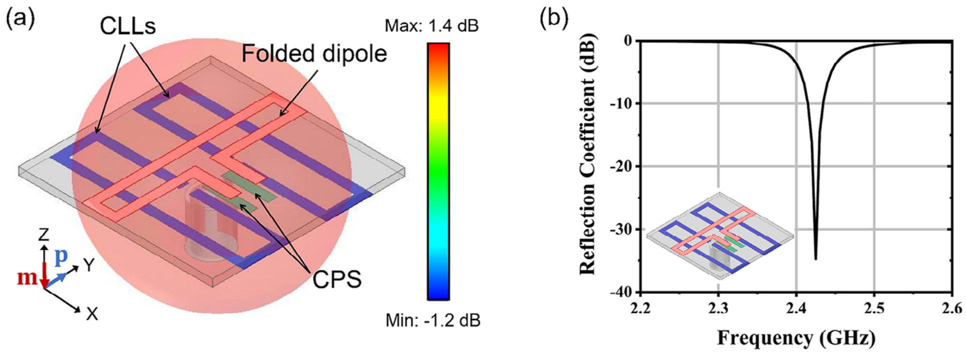

Figure 2. a) A diagram of the Janus antenna (quasi-isotropic electrically small antenna) composed of the folded dipole, capacitively loaded loops (CLLs) and driven coplanar stripline section (CPS). The 3D radiation pattern of the Janus antenna is shown to be quasi-isotropic. b) The reflection coefficient of the Janus antenna.

performance and the theoretical far-field pattern of the Janus source. Details on the latter can be found in Note S1 (Supporting Information).

We now examine the electromagnetic near-fields of the Janus antenna. **Figure** 3a plots the distribution of the electric field near the Janus antenna. The inset shows the vectorial field distribution on the x-y-plane. The electric field points strongly in the $+y$-direction as indicated by the red arrow. Similarly, Figure 3b shows the magnetic field distribution in the near-field, which indicates that the magnetic field points predominantly in the $-z$-direction

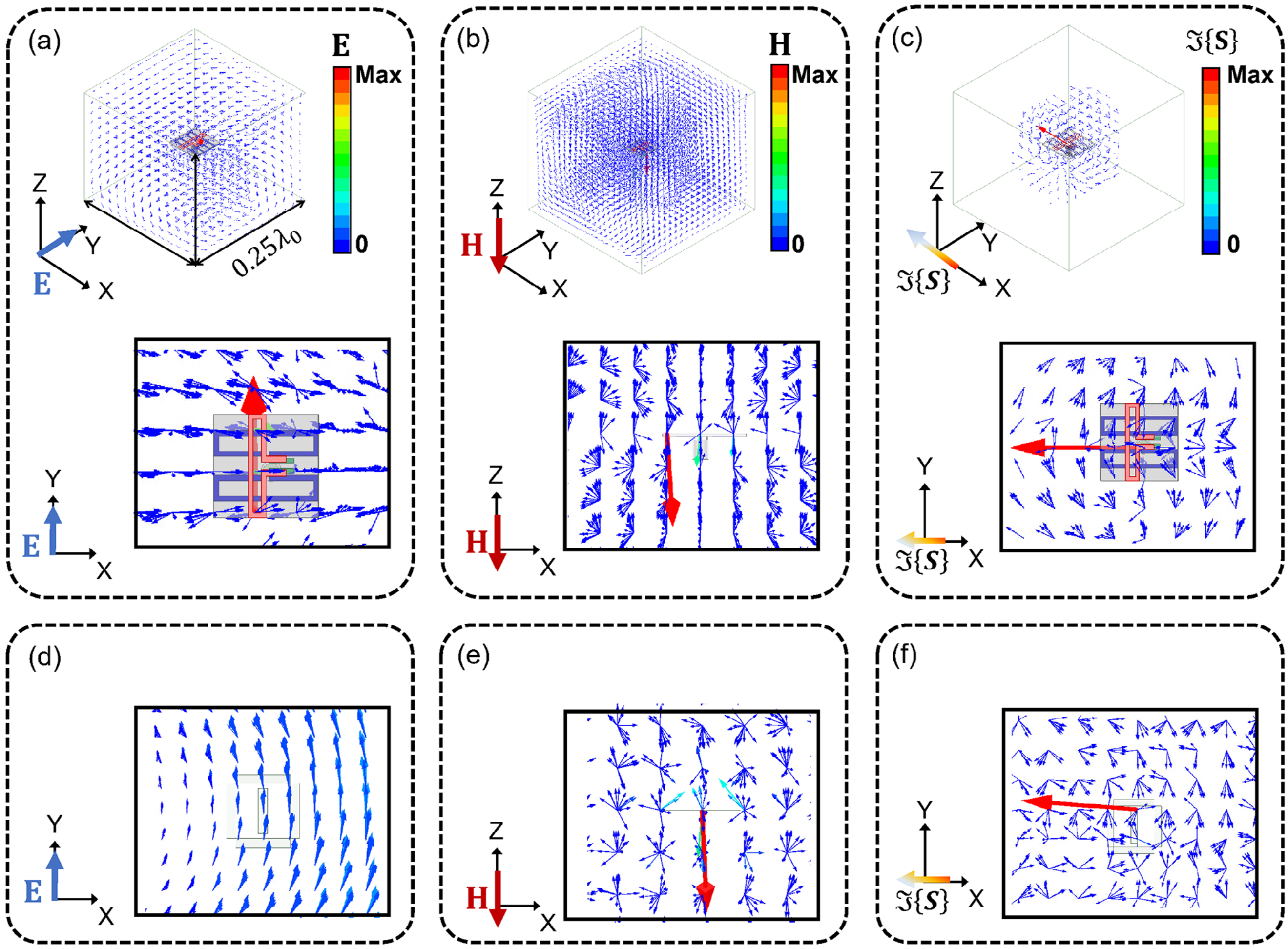

Figure 3. The vector plot of the simulated Janus antenna's a) electric field, b) magnetic field and c) imaginary part of the Poynting vector. The vector plot of the ideal Janus source's d) electric field, e) magnetic field and f) imaginary part of the Poynting vector.

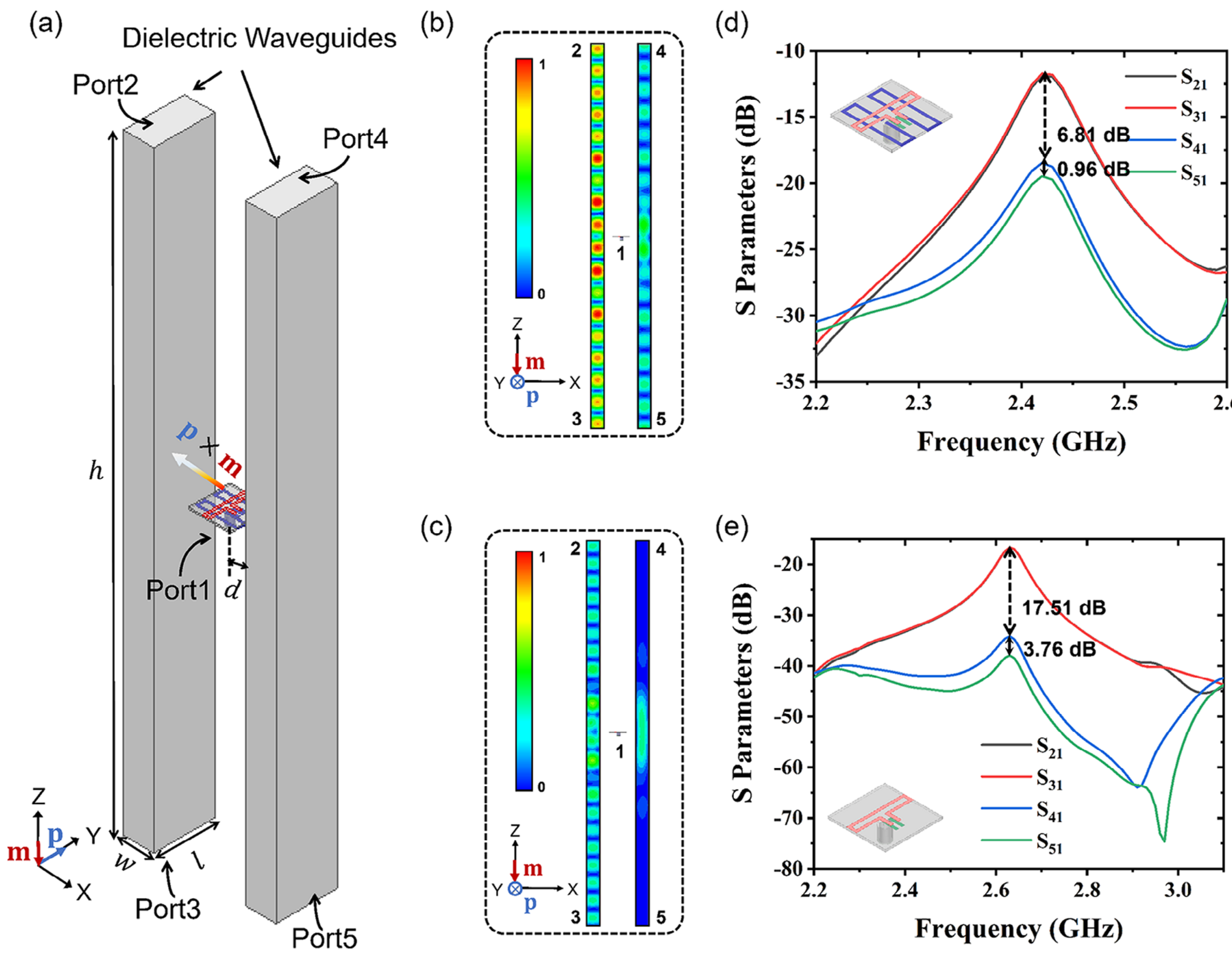

Figure 4. a) A schematic of the Janus antenna with dielectric waveguides. The dielectric waveguide dimensions are $h = 620$ mm, $l = 30$ mm, $w = 15$ mm and $d = 15$ mm ($0.12\ \lambda_0$). Simulated near-field directionality of b) Janus antenna and c) optimized Janus antenna. Coupling coefficients (S_{21}, S_{31}, S_{41}, S_{51}) with respect to frequency of d) Janus antenna and e) optimized Janus antenna.

in close proximity to the Janus antenna. Finally, Figure 3c illustrates the imaginary part of the Poynting vector in the near-field region, showing that it is pointing predominantly toward the -x-direction. These directional tendencies are in agreement with the theoretically calculated field distributions from an ideal Janus source, which we plot for comparison in Figure 3d–f. The theoretical Janus source is constructed with ideal current strips and current loops with suitable amplitude relations as developed.[19,22] More details are given in Note S1 (Supporting Information). The results show that the near-field of this antenna indeed matches the expected near-field of a Janus source.

We now investigate the Janus antenna's directionality in a waveguide coupling scenario, following. [1] As illustrated in **Figure 4**a, the Janus antenna is strategically sandwiched between two dielectric waveguides, with dimensions $h = 620$ mm, $l = 30$ mm, $w = 15$ mm. The separation between the edges of the antenna and the adjacent waveguides is $d = 15$ mm ($0.12\ \lambda_0$). In this situation, the near-field characteristic of the antenna manifests through the interaction of its near-field and the dielectric waveguides. The interaction is calculated as $|\mathbf{p}\cdot\mathbf{E}^* + \mathbf{m}\cdot\mathbf{B}^*|$, where $\mathbf{p}$ is the electric dipole moment, $\mathbf{m}$ is the magnetic dipole moment, $\mathbf{E}$, and $\mathbf{B}$ are the electric and magnetic fields of the dielectric normalized waveguide mode at the location of the Janus dipole. In order to improve the near-field directionality, we optimize the strengths of the magnetic and electric dipole moments of the Janus antenna such that $|\mathbf{p}\cdot\mathbf{E}^* + \mathbf{m}\cdot\mathbf{B}^*| = 0$ for the weak-coupling side, following.[1] Interestingly, we find that a folded dipole, which inherently combines an electric dipole and a magnetic dipole, serves well as an optimized Janus antenna in our situation. The resonance frequency of the optimized Janus antenna shifts slightly to 2.63 GHz.

Figure 4b,c shows the waveguide coupling simulation results for both the Janus antenna and the optimized Janus antenna, respectively. It can be seen that the Janus antenna predominantly excites the waveguide in the -x direction, which is consistent with its directionality as inferred from the imaginary part of the Poynting vector. However, as illustrated in Figure 4b, the (unoptimized) Janus antenna's near-field directionality is not that high, as evidenced by appreciable coupling to the waveguide to the +x direction. In contrast, the optimized Janus antenna, as depicted in

Figure 4c, boasts remarkable near-field directionality. In this configuration, power from the Janus antenna couples to the waveguide on one side only, and the Janus antenna-waveguide system possesses superb near-field directionality. We use microwave network theory to quantitatively examine the near-field directionality. We designate the antenna excitation as Port 1, and the ends of the two waveguides as Ports (2, 3) and Ports (4, 5), respectively. The parameter S_{i1} denotes the ratio of the power wave exiting Port i to the power wave incident at Port 1.

Figure 4d,e shows the power coupled to the 4 waveguide ports as a function of frequency. Figure 4d shows that when the Janus antenna is placed between the dielectric waveguides, the two ports connected to the coupled waveguide (Ports 2 and 3) receive similar amounts of power, while the two ports connected to the uncoupled waveguide (Ports 4 and 5) receive a lot less power. A similar result is observed in Figure 4e when the optimized Janus antenna is placed between the dielectric waveguides, but the directionality is improved to more than 17 dB (more than 50-fold difference in power). The slight difference in the received powers of Ports 4 and 5 in Figure 4e is the result of the slight circuit asymmetry of the Janus antennas and the precision limitation of the full-wave simulation.

To encapsulate the achieved the near-field directionality of the Janus antenna, we define a figure of merit, which is the ratio of the average wave amplitude coupled to the two preferred ports, to the average wave amplitude coupled to the two unpreferred ports:

$$D_{NF} = \left(|S_{21}| + |S_{31}|\right) \ / \left(|S_{41}| + |S_{51}|\right) \tag{1}$$

Using Equation (1), we find that the near-field directionalities for the Janus and optimized Janus antennas are 7.36 and 19.39 dB, respectively. Moreover, we observe that both the Janus and the optimized Janus antennas maintain excellent near-field directionality over a wide bandwidth: a 3 dB near-field directionality is achieved from 2.3 to 2.59 GHz (11.93% bandwidth) for the Janus antenna and from 2.28 to 3.04 GHz (28.9% bandwidth) for the optimized Janus antenna. Obtaining strong directionality over a large bandwidth bodes well for the Janus antenna's potential as a near-field directional switch.

Further, the efficiency of the proposed Janus antenna can be significantly improved since it is active. We compare the efficiency of the passive Janus source proposed in our previous work[20] with the Janus antenna in this work. Figure S2 (Supporting Information) shows the excitation and coupling set-ups for the passive and active Janus sources. For the passive Janus source in Figure S2a (Supporting Information), a horn antenna emits a Gaussian beam with the necessary incidence and polarization angles to excite the Janus source. The separation distance between the horn and the Janus source is 500 mm: a shorter separation distance is insufficient to reach the antenna far-zone and may interfere with other parts of the experimental setup. For the active Janus source in Figure S2b (Supporting Information), the Janus antenna, fed by a coaxial cable, replaces the passive Janus source and the horn antenna. The simulation results show that, when Port 1 is excited with the power of 1 W, 2.4 mW is coupled into Port 2 (one of the ports preferred by the Janus source) for the passive Janus setup, while 250 mW is coupled into Port 2 for the Janus antenna setup. Thus, the near-field coupling of

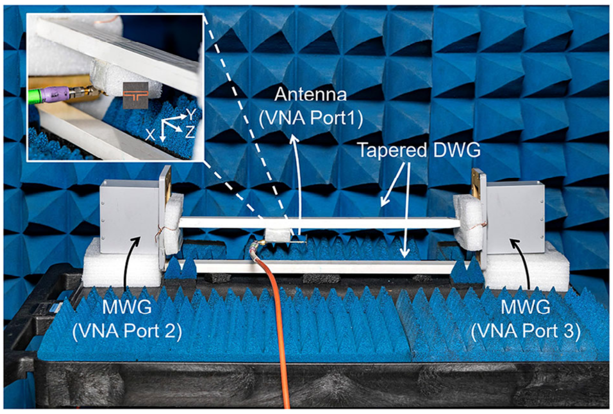

Figure 5. A diagram of the experiment setup. The (optimized) Janus antenna is connected to Port 1 of a Vector Network Analyzer (VNA). The tapered dielectric waveguide (DWG) transitions into two Metallic Waveguides (MWGs) at both ends. The MWGs are connected to Ports 2 and 3 of the VNA, respectively.

the Janus antenna improves the efficiency by a factor of 105 compared to that of the passive Janus source. Similarly, as shown in Figure S2c (Supporting Information), 147 mW is coupled into Port 2 for the optimized Janus antenna. Hence the power efficiency is 61 times that of the passive Janus source. This dramatic improvement in coupling efficiency makes the Janus antenna an efficient device for investigating near-field directionality effects and building practical power-coupling switches.

3. Experimental Demonstration

We proceeded to experimentally demonstrate the near-field directional coupling of the Janus antenna. **Figure 5** shows a photograph of the experimental setup. We excited, at Port 1, the test antenna, which was either a Janus antenna or an optimized Janus antenna. The near-field of the Janus antenna will interact, and couple into the rectangular dielectric waveguides on either side of the Janus antenna. The dimensions of the waveguides and their separation distance were as reported in the section on full-wave simulation. The antenna was oriented such that optimal coupling was achieved in the *-x* direction. WR430 waveguide launchers were positioned at the ends of each dielectric waveguide to measure power transmitted into the waveguides. The dielectric waveguides were tapered at the ends to optimize coupling into the WR430 launchers. We connected two launchers first to Ports 2 and 3, then to Ports 4 and 5, to measure power coupled to each waveguide. At each step, we terminated the other waveguide ports using microwave absorbers to prevent unwanted backreflections. The Note S3 (Supporting Information) shows that waves can be coupled into the WR430 launchers and absorbed by the absorbers with near-perfect efficiency and minimal reflection at the end of the waveguide. We connected the transmit (Port 1) and receive ports (Ports 2 and 3, and then Ports 4 and 5) to a vector network analyzer which measures the S-parameter over a broad bandwidth. The experiment takes place within an antenna chamber that absorbs the wave radiated by the Janus antenna, thus eliminating spurious reflection by the walls of the test chamber.

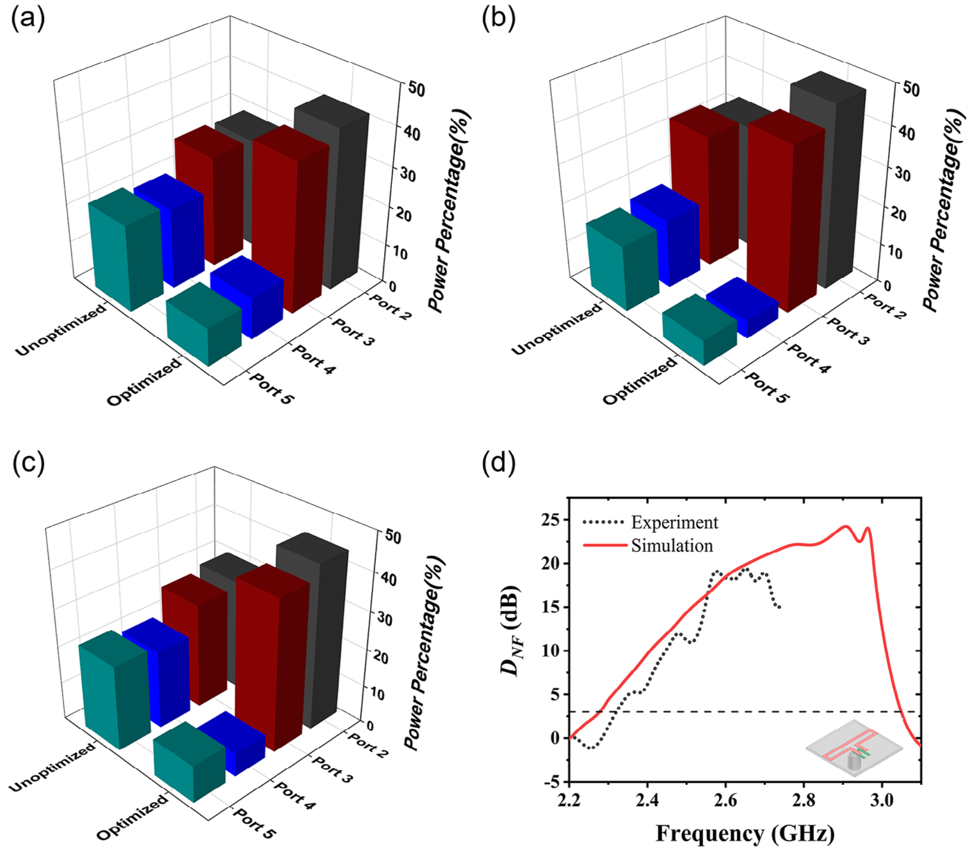

Figure 6. The power percentage distribution of the Janus antenna and the optimized Janus antenna's Ports 2–5 at different frequencies a) f_L_unoptimized =2.33 GHz, f_L_optimized =2.53 GHz, b) f_0_unoptimized =2.43 GHz, f_0_optimized =2.63 GHz, c) f_H_unoptimized =2.53 GHz, f_H_optimized =2.73 GHz. d) The measured and simulated near-field directionality D_{NF} (dB) of the optimized Janus antenna with respect to frequency.

Figure 6a–c shows the experimental results at the resonance frequencies of both the unoptimized and optimized Janus antennas (f_0_unoptimized =2.43 GHz, f_0_optimized =2.63 GHz), as well as frequencies 0.1 GHz below and above the respective resonances. The black and red bars show the received power (%) of the coupled ends (i.e., Ports 2 and 3), while the blue and green bars represent the received power (%) of the uncoupled ends (i.e., Ports 4 and 5). It can be clearly seen that more power flows into the coupled waveguide compared to the uncoupled waveguide. In the same way, the sum of the energies of the two ports of the coupled waveguide was divided by the sum of the energies of the two ports of the uncoupled waveguide, i.e., the corresponding experiment near-field directionality. **Table** 1 tabulates the near-field directionalities, as calculated from applying Equation (1) onto the experimentally obtained S-parameters. The table also provides a comparison with the simulated directionalities. It was observed that at the central operation frequency f_0, both Janus antennas can obtain reasonable directionalities. In particular, optimized Janus antenna can achieve an experimental directionality of 17.94 dB ($D_{NF} = 7.9$), meaning 98.4% of the power was coupled to the preferred waveguide. Moreover, at $f_L = 2.53$ GHz and $f_H = 2.73$ GHz, the optimized Janus antenna achieves a directionality of over 10 dB, meaning that over this bandwidth, over 90.9% of the power was coupled to the preferred waveguide. Figure 6d shows the measured and simulated near-field directionality of the optimized Janus antenna as a function of frequency. It can be seen that the simulated and experimental directionalities agree well with one another up to 2.74 GHz, which was the upper-frequency limit for the WR430 waveguide launcher. A maximum directionality of 19.62 dB ($D_{NF} = 9.6$) has been experimentally demonstrated. The measured 3 dB directionality bandwidth was 16.3%, which can already be considered wideband for practical applications; however, the excellent agreement in Figure 6d suggests that, with proper waveguide launchers, an operation bandwidth similar to the simulated bandwidth (28.9 %) can be achieved. Slight simulation-experiment discrepancy comes from i) the antenna's narrow impedance bandwidth and ii) experimental limitations such as small free-space

Table 1. Simulated and measured near-field directionality (dB) of the unoptimized and optimized Janus antenna for three frequencies (low frequency f_L, center frequency f_o and high frequency f_H).

		f_L	f_0	f_H
Unoptimized Janus Antenna	Simulated	4.52	7.36	7.78
	Measured	2.38	5.47	2.41
Optimized Janus Antenna	Simulated	15.62	19.39	21.48
	Measured	11.76	17.94	14.40

reflections and imperfect waveguide-to-cable coupling at the waveguide taper and launchers.

4. Conclusion

In this paper, we experimentally demonstrate a 3D active Janus source that achieves broadband near-field directionality modulation with significantly enhanced power efficiency compared to existing passive Janus sources. Specifically, the proposed Janus antenna attains a 3-dB near-field directionality over a 28.9% bandwidth, with power efficiency improvements exceeding 60 times that of passive sources. Our work not only elucidates the connection between the "Janus dipole" concept in physics and the "quasi-isotropic antenna" concept in antenna engineering, but also paves the way for the development of future directional devices with vastly improved bandwidth and efficiency. This advancement holds the potential to revolutionize the design and application of antennas in various near-field applications like efficient wireless power transfer, asymmetric coupling, and wave routing in sub-wavelength compact systems, among many others. Particularly, we envisage that the quasi-isotropic far-field radiation and the near-field directionality of the Janus source can be leveraged to build compact MIMO systems with greatly reduced inter-element coupling and wireless power transfer systems with enhanced inter-element coupling.

Supporting Information

Supporting Information is available from the Wiley Online Library or from the author.

Acknowledgements

The work described in this paper was supported by the Government of Hong Kong's RGC General Research Fund (CityU 11204522).

Conflict of Interest

The authors declare no conflict of interest.

Data Availability Statement

The data that support the findings of this study are available from the corresponding author upon reasonable request.

Keywords

directionality, Janus source, metamaterial, near-field coupling, quasi-isotropic antenna

Published online: September 23, 2024

[1] M. F. Picardi, A. V. Zayats, F. J. Rodríguez-Fortuño, *Phys. Rev. Lett.* **2018**, *120*, 117402.
[2] K. Yao, Y. Liu, *ACS Photonics* **2016**, *3*, 953.
[3] Y. H. Fu, A. I. Kuznetsov, A. E. Miroshnichenko, Y. F. Yu, B. Luk'yanchuk, *Nat. Commun.* **2013**, *4*, 1527.
[4] R. W. Ziolkowski, *Phys. Rev. X* **2017**, *7*, 031017.
[5] K.-M. Luk, H. Wong, *Int. J. Microw. Opt. Technol.* **2006**, *1*, 35.
[6] R. W. Ziolkowski, *IEEE Access* **2015**, *3*, 2644.
[7] M. Chen, M. Kim, A. M. H. Wong, G. V. Eleftheriades, *Nanophotonics* **2018**, *7*, 1207.
[8] C. Pfeiffer, A. Grbic, *Phys. Rev. Lett.* **2013**, *110*, 197401.
[9] M. Picardi, A. Zayats, F. Rodríguez-Fortuño, *Europhys. News* **2018**, *49*, 14.
[10] M. F. Picardi, M. Neugebauer, J. S. Eismann, G. Leuchs, P. Banzer, F. J. Rodríguez-Fortuño, A. V. Zayats, *Light Sci Appl* **2019**, *8*, 52.
[11] Y. Long, H. Ge, D. Zhang, X. Xu, J. Ren, M.-H. Lu, M. Bao, H. Chen, Y.-F. Chen, *Natl Sci Rev* **2020**, *7*, 1024.
[12] Y. Long, J. Ren, Z. Guo, H. Jiang, Y. Wang, Y. Sun, H. Chen, *Phys. Rev. Lett.* **2020**, *125*, 157401.
[13] L. Wei, F. J. Rodríguez-Fortuño, *New J. Phys.* **2020**, *22*, 083016.
[14] L. Wei, F. J. Rodríguez-Fortuño, *Phys. Rev. Appl.* **2020**, *13*, 014008.
[15] T. Wu, A. Baron, P. Lalanne, K. Vynck, *Phys. Rev. A* **2020**, *101*, 011803.
[16] Y. Jiang, X. Lin, H. Chen, *Prog. Electromagn. Res.* **2021**, *170*, 169.
[17] Y. Zhong, X. Lin, J. Jiang, Y. Yang, G.-G. Liu, H. Xue, T. Low, H. Chen, B. Zhang, *Laser Photonics Rev.* **2021**, *15*, 2000388.
[18] M. F. Picardi, C. P. T. McPolin, J. J. Kingsley-Smith, X. Zhang, S. Xiao, F. J. Rodríguez-Fortuño, A. V. Zayats, *Appl. Phys. Rev.* **2022**, *9*, 021410.
[19] B. Xue, A. M. H. Wong, in 2022 IEEE Int. Symp. Antennas Propag. USNC-URSI Radio Sci. Meet. AP-SURSI **2022**, pp. 974, https://doi.org/10.1109/AP-S/USNC-URSI47032.2022.9886451.
[20] Y. Cheng, K. A. Oyesina, B. Xue, D. Lei, A. M. H. Wong, S. Wang, *Proc. Natl. Acad. Sci.* **2023**, *120*, e2301620120.
[21] C. Bian, Y. Zhong, X. Chen, T. Low, H. Chen, B. Zhang, X. Lin, *Phys. Rev. A* **2024**, *109*, 033505.
[22] B. Xue, K. A. Oyesina, A. M. H. Wong, *Commun. Phys.* **2024**, *7*, 87.
[23] Y. Zhong, C. Wang, C. Bian, X. Chen, J. Chen, X. Zhu, H. Hu, T. Low, H. Chen, B. Zhang, X. Lin, *Opt. Lett.* **2024**, *49*, 826.
[24] P. Yu, J. Li, S. Zhang, Z. Jin, G. Schütz, C.-W. Qiu, M. Hirscher, N. Liu, *Nano Lett.* **2018**, *18*, 4584.
[25] K. Chen, G. Ding, G. Hu, Z. Jin, J. Zhao, Y. Feng, T. Jiang, A. Alù, C.-W. Qiu, *Adv. Mater.* **2020**, *32*, 1906352.
[26] S. J. Li, Y. B. Li, H. Li, Z. X. Wang, C. Zhang, Z. X. Guo, R. Q. Li, X. Y. Cao, Q. Cheng, T. J. Cui, *Ann. Phys.* **2020**, *532*, 2000020.
[27] B. Chen, S. Yang, J. Chen, J. Wu, K. Chen, W. Li, Y. Tan, Z. Wang, H. Qiu, K. Fan, C. Zhang, H. Wang, Y. Feng, Y. He, B. Jin, X. Wu, J. Chen, P. Wu, *Light Sci Appl.* **2023**, *12*, 136.
[28] H. Tang, C. J. Bulger, T. Rovere, B. Zheng, S. An, H. Li, Y. Dong, M. Haerinia, C. Fowler, S. Gonya, W. Guo, H. Zhang, *IEEE Antennas Wirel. Propag. Lett.* **2023**, *22*, 49.
[29] Y.-M. Pan, K. W. Leung, K. Lu, *IEEE Trans. Antennas Propag.* **2014**, *62*, 577.
[30] P. F. Hu, Y. M. Pan, X. Y. Zhang, B. J. Hu, *IEEE Trans. Antennas Propag.* **2019**, *67*, 1294.
[31] C.-H. Wu, T.-G. Ma, *IEEE Trans. Antennas Propag.* **2014**, *62*, 933.
[32] J.-H. Kim, S. Nam, *IEEE Antennas Wirel. Propag. Lett.* **2017**, *16*, 294.
[33] J. Ouyang, Y. M. Pan, S. Y. Zheng, P. F. Hu, *IEEE Antennas Wirel. Propag. Lett.* **2018**, *17*, 303.
[34] Y. Wang, M.-C. Tang, S. Chen, L. Li, D. Li, K.-Z. Hu, M. Li, *IEEE Antennas Wirel. Propag. Lett.* **2019**, *18*, 1646.
[35] S. M. Radha, G. Shin, W. Kim, S. I. H. Shah, I.-J. Yoon, *IEEE Antennas Wirel. Propag. Lett.* **2020**, *19*, 2482.
[36] Y. Xu, Y. Zhu, S. Wen, Y. Dong, *IEEE Antennas Wirel. Propag. Lett.* **2021**, *20*, 2407.
[37] Y. Wang, M.-C. Tang, T. Shi, D. Yi, D. Li, X. Zeng, *IEEE Trans Antennas Propag* **2022**, *70*, 11559.